applied sciences

MDPI

Article

Silica Microsphere WGMR-Based Kerr-OFC Light Source and Its Application for High-Speed IM/DD Short-Reach Optical Interconnects

Toms Salgals [1,2,*], Janis Alnis [3], Oskars Ozolins [1,4,5], Alexey V. Andrianov [6], Elena A. Anashkina [6], Inga Brice [3], Roberts Berkis [3,7], Xiaodan Pang [1,5], Aleksejs Udalcovs [1], Jurgis Porins [1], Sandis Spolitis [1,8] and Vjaceslavs Bobrovs [1]

1 Institute of Telecommunications, Riga Technical University, 12 Azenes Street, 1048 Riga, Latvia; ozolins@kth.se (O.O.); xiaodan@kth.se (X.P.); aleksejs.udalcovs@gmail.com (A.U.); jurgis.porins@rtu.lv (J.P.); sandis.spolitis@rtu.lv (S.S.); vjaceslavs.bobrovs@rtu.lv (V.B.)
2 AFFOC Solutions Ltd., 17 Andrejostas Street, 1045 Riga, Latvia
3 Institute of Atomic Physics and Spectroscopy, University of Latvia, 3 Jelgavas Street, 1004 Riga, Latvia; janis.alnis@lu.lv (J.A.); inga.brice@lu.lv (I.B.); roberts.berkis@uibk.ac.at (R.B.)
4 Networks Unit, RISE Research Institutes of Sweden, Kista, 164 40 Stockholm, Sweden
5 Applied Physics Department, KTH Royal Institute of Technology, 106 91 Stockholm, Sweden
6 Institute of Applied Physics of the Russian Academy of Sciences, 46 Ul'yanov Street, 603950 Nizhny Novgorod, Russia; alex.v.andrianov@gmail.com (A.V.A.); elena.anashkina@gmail.com (E.A.A.)
7 Institute for Experimental Physics, University of Innsbruck, Technikerstrasse 25, 6020 Innsbruck, Austria
8 Communication Technologies Research Center, Riga Technical University, 12 Azenes Street, 1048 Riga, Latvia
* Correspondence: toms.salgals@rtu.lv; Tel.: +371-278-36-269

Citation: Salgals, T.; Alnis, J.; Ozolins, O.; Andrianov, A.V.; Anashkina, E.A.; Brice, I.; Berkis, R.; Pang, X.; Udalcovs, A.; Porins, J.; et al. Silica Microsphere WGMR-Based Kerr-OFC Light Source and Its Application for High-Speed IM/DD Short-Reach Optical Interconnects. *Appl. Sci.* **2022**, *12*, 4722. https://doi.org/10.3390/app12094722

Academic Editors: (John) Xiupu Zhang and Gaoming Xu

Received: 18 March 2022
Accepted: 3 May 2022
Published: 7 May 2022

Abstract: Kerr optical frequency combs (OFCs) based on silica microsphere whispering gallery mode resonator (WGMR) have various applications where they are used as a light source. For telecommunication purposes, WGMR-based Kerr-OFC comb generators can be physically realized using silica microsphere resonators and can be used to replace multiple laser arrays. In such a realization, these novel light sources have the potential to demonstrate an attractive solution for intra-datacenter interconnects (DCI). In this paper, we show an experimental demonstration of a silica microsphere WGMR-based Kerr OFC light source where newly generated 400 GHz spaced carriers together with powerful linear equalization techniques, such as a linear symbol-spaced adaptive decision-feedback equalizer (DFE) with feed-forward (FF) and feedback (FB) taps, provide an alternative to individual lasers ensuring low-cost and low-complexity IM/DD scheme for the transmission of NRZ-OOK modulated signals at data rates up to 50 Gbps/λ over 2 km SMF link. Finally, we demonstrate a record 50 Gbps per λ transmission of NRZ-OOK modulated signals with a novel silica microsphere WGMR-based Kerr-OFC as a light source operating in the optical C-band, surpassing the previously demonstrated data rate record by five times.

Keywords: Kerr optical frequency combs (OFC); silica microsphere; intra-datacenter interconnects (DCI); equalization

1. Introduction

Kerr optical frequency combs (OFC) based on whispering-gallery-mode microresonator (WGMR) with a single laser source have already shown different applications and especially its application in fiber optical communication systems replacing multiple laser arrays [1]. Accurate timing, low phase noise, and the narrow linewidth of generated harmonics allow achieving the ultimate performance desired from an optical comb-based system. In addition, OFC generators have applications in areas such as optical clocks [2],

ultra-stable microwave generators [3], applications that require a precise and stable optical frequency distribution via long fiber [4], spectroscopy [5], sensing [6], quantum applications [7], optical communications [8], etc. OFC sources for wavelength division multiplexed (WDM) systems cover use cases ranging from short reach fiber-optic links (e.g., as for data center interconnects (DCI)) to metro-access fiber-optic links interconnecting large geographic areas [9,10]. More specifically, the WGMR-based Kerr-OFC comb generators physically realized on silica microsphere demonstrate [9] a new concept able to provide an attractive solution to intra-DCIs due to low costs and energy consumption. The data centers (DCs) are the foundation of Internet applications such as cloud computing, where Big Data storage and large-scale high-performance computing (HPC) take place. The intra-DCI devices require not only large capacity but, most importantly, high scalability and low energy consumption. Therefore, these requirements require new transmission technologies for short-reach communications [10,11].

It can provide a lower energy consumption while ensuring improved spectral efficiency and a stable frequency spacing between OFC lines (carriers) thanks to the sustained strong phase relation between them [9,12,13]. OFCs have various realizations; among them, the realization by four-wave mixing (FWM) in highly nonlinear optical fiber (HNLF) [13], electro-optic phase modulation of a laser using, e.g., cascaded phase and amplitude modulators [1,14], chip-based mode-locked laser (MLL) combs [13], and silicon microroring resonators [13,15]. Potentially cost-effective solutions for the realization of data transmission in optical WDM networks are OFC generation in silica whispering gallery mode resonator–microspheres manufactured from melted telecom fiber, e.g., from Corning SMF 28e (ITU-T G.652) [9,12,14], which is realized as the pumping of a high-quality (high Q factor) optical resonator with Kerr nonlinearity using a single continuous-wave (CW) laser. When optimal conditions are met, the intracavity pump photons are redistributed via the FWM to the neighboring cavity modes, thereby creating the so-called Kerr OFC. The exciting pump signal is launched into the Kerr-OFC resonator via a tapered fiber, and an OFC is generated at the output of this taper. In addition to being energy-efficient, conceptually simple and structurally robust Kerr comb generators are very compact devices (to micrometric size) that can be integrated on a chip [16,17]. Kerr microresonator OFCs can achieve bandwidths of hundreds of nanometers covering different (e.g., E-, S-, C-, and L-band) telecommunication bands (according to ITU-T G. 694.1 recommendation) [18,19].

Considering the findings of our previous works [9,12,20,21], here, we propose a silica microsphere WGMR-based Kerr-OFC as a light source operating in the C-band (1530–1565 nm) and having 400 GHz spaced comb lines. These comb lines are subsequently used as optical carriers for the data transmission using the intensity modulation direct detection (IM/DD). Data rates up to 50 Gbps/λ are employed in combination with the non-return to zero (NRZ) on-off keying (OOK) format for the transmission over a 2 km short fiber-optic link consisting of the standard ITU-T G.652 single-mode fiber. The aforementioned IM/DD signal format is chosen as it still dominates in short-reach optical interconnects due to its simplicity. Digital equalization techniques shown in our previous works [22], such as a linear equalizer with feed-forward (FF) and feedback (FB) taps, can improve the signal quality due to different system distortions, mainly caused by limited channel bandwidth and nonlinearities during the optical to electrical (O/E) and electrical to optical (E/O) conversions and the link induced inter-symbol interference (ISI). Therefore, we apply the use of the symbol-spaced adaptive decision-feedback equalizer (DFE) implemented at the receiver part to improve the pre-FEC bitrate and to achieve higher data rates in DCI with the optical carriers generated by the developed silica microsphere WGMR-based Kerr-OFC.

The rest of the paper is structured as follows. Section 2 describes the characteristics of the designed silica microsphere and shows the deterioration of its Q factor with time. Section 3 presents the experimental setup of the WGMR-based Kerr-OFC light source operating in the C-band and used for the generation of 400 GHz spaced optical carriers. This

section also describes the fabrication process of a tapered fiber used for the coupling of light into and out of a silica microsphere and the experimental setup used to characterize coupling conditions between the silica microsphere and the tapered fiber. Furthermore, Section 3 reveals the experimentally obtained characteristics of the designed WGMR-based Kerr-OFC light source, Q factor, and optical output spectra. Section 4 summarizes the conducted data transmission experiment by analyzing the received signal bit error rates (BER) and eye diagrams. The impact that digital post-equalization at the receiver has on system performance is provided in Section 5. Finally, Section 6 overviews the experimental results and concludes the paper.

2. Characteristics of Designed Silica Microsphere WGMR for Kerr-OFC

Silica (SiO_2) microspheres with a diameter of D = 170 μm used for the Kerr-OFC were fabricated from a standard ITU-T G.652 single-mode telecommunication fiber by the melting method using a specially developed program for a commercially available optical fusion arc splicer, which has been previously demonstrated by authors in [9,23]. During the manufacturing process, by changing the diameter of the fabricated silica microsphere, we can obtain an OFC with a free spectral range (FSR) ranging from about 200 GHz (sphere D = 320 μm) [20] up to about 400 GHz (sphere D = 170 μm) [18] in addition to the possibility of finetuning the coupling conditions between the resonator and tapered fiber, which is not possible for chip-based resonators with integrated waveguides, and therefore can be considered to be a major advantage over other OFC technologies. Silica microsphere resonators also have advantages of fast and simple fabrication using commercially available fusion arc splicers, allowing the fabrication of silica microspheres with user-defined sphere diameter and high-quality factor ($Q \geq 10^7$) in a couple of minutes.

Most applications, especially silica microsphere-based Kerr-OFC, require the realization of the highest possible quality factor (so-called Q factor) microsphere resonators. In regular laboratory conditions, the microsphere's Q factor deteriorates within a 1 h time scale in the open environment due to the deposition of nanoscale particles or water vapors to the microsphere surface. The Q factor of the microsphere is determined by several aspects such as intrinsic radiative (curvature) losses, scattering losses on residual surface inhomogeneities, losses introduced by surface contaminants, and material losses [24]. For a more detailed illustration, see Figure 1 where newly fabricated and artificial degradations of the microsphere surface by water vapors are obtained using a scanning electron microscope (SEM, Hitachi S-4800) for 170 μm silica microsphere resonators. Scanned sphere illustrations with a focused beam of electrons (captured at: 3 kV (accelerating voltage) and 4.0 mm (surface scale) @ ×400 to 45.0 k times and 2.9 mm @ ×180 k times) for a particular micro-sphere resonator after 100% humidity exposure (resonator has been in humidity fog for 5 s) are shown in Figure 1a–d. The newly fabricated silica microsphere resonator obtained by SEM (captured at: 3 kV, 4.0 mm @ ×300 to 50.0 k times) is shown in Figure 1e–h. White dots (see Figure 1f) for evaporated silica (cristobalite) from the arc fusion splicer discharge explain why the maximal Q factor of a newly fabricated microsphere is below 1×10^8. We can observe that the evaporated silica dust from the arc fusion splicer (see Figure 1g) and nanoscale particles (see Figure 1h) are deposited on the surface of the silica microsphere.

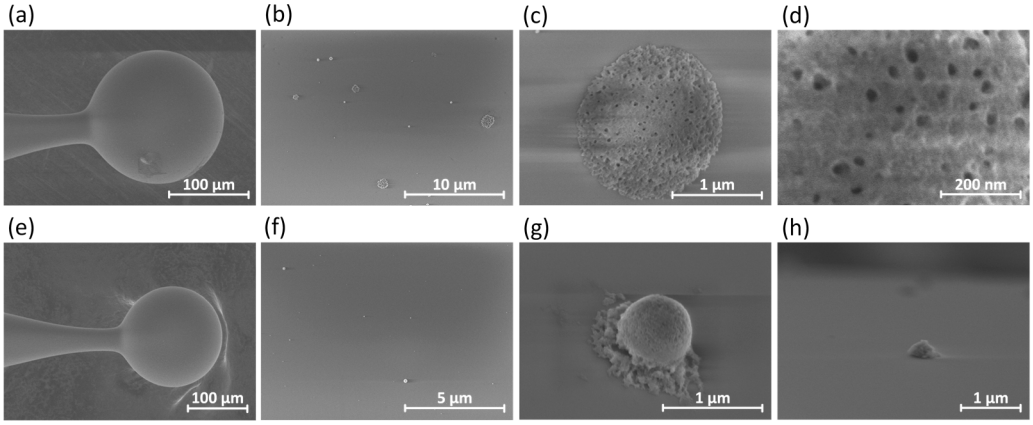

Figure 1. Illustration of 170 µm SiO_2 microsphere resonator scans captured by SEM at 3 kV after artificial degradation by 100% humidity exposure: (**a**) 4.1 mm @×400 times, (**b**) 4.0 mm @×5.00 k times, (**c**) 4.0 mm @×45.0 k times, (**d**) 2.9 mm @×180 k times, and captured illustrations for newly fabricated 170 µm SiO_2 microsphere: (**e**) 4.0 mm @×300 times, (**f**) 4.0 mm @×10.0 k times, (**g**) where evaporated silica from the arc fusion splicer discharge at 4.0 mm @×50.0 k times, and (**h**) nanoscale particles at 4.0 mm @×30.0 k times were observed.

It is important to note that, during the experiment, by testing samples of fabricated microspheres, we were able to significantly improve the degraded 4-month-old microsphere (added by water vapor) Q factor from Q = 2.0 × 10^6 (96 MHz full width at half maximum (FWHM) of the WGM resonance) to Q = 4.4 × 10^6 (44 MHz FWHM of the WGM resonance) using pure hydrogen (H) flame of a micro burner. Note that the Q factor of the newly fabricated microsphere was 3.7 × 10^7 (5.2 MHz FWHM of the WGM resonance). The built-up circulating intensity [25] was estimated to be 14 GW/cm^2 exceeding ~2.0 GW/cm^2 [26] needed for OFC generation (see Table 1). No OFC was generated when it degraded below 2.0 GW/cm^2. Microresonator with high Q factor can build up a significant internal circulating intensity when pumped with low laser power. The circulating intensity can be found using the following equation [25]:

$$I_{circ} = \frac{P_{circ}}{A_{eff}}, \quad (1)$$

where P_{circ} is internal circulating power, and A_{eff} is the effective area of the mode area of the resonance. A_{eff} can be found by using simulations. As calculation parameters, resonator radius, refraction index, and resonance frequency at 1550 nm wavelength for fundamental mode were used. P_{circ} in the silica microsphere WGMR can be found as follows [25]:

$$P_{circ} = P_{in} \frac{\lambda Q_{intr}}{\pi^2 nR} \frac{K}{(K+1)^2}, \quad (2)$$

where λ is the resonance wavelength, n is the refraction coefficient, R is the microsphere radius, P_{in} is the input power (P_{in} = 100 mW), $K = Q_{intr}/Q_{extr}$ is the coupling parameter that shows the ratio between intrinsic and extrinsic Q-factors, and Q_{intr} is the intrinsic Q factor, which is limited by all losses defined by the resonator cavity. The coupling parameter can be estimated using transmission T at the resonance frequency [27].

$$T = \left(\frac{1-K}{1+K}\right)^2 \text{ or } K = \frac{1 \pm \sqrt{T}}{1 \mp \sqrt{T}}., \quad (3)$$

Several moisture and dust degradation methods of protection can be used to keep high Q factor of newly fabricated silica resonators, for instance, storage with ethanol drops or storage with dry nitrogen within hermetic enclosure boxes. The packaging technique utilized by UV-curable polymer for stabilizing both the microsphere and the tapered fiber could be preferred for long-term maintenance of silica microsphere WGMR-based Kerr-OFC light sources. While the use of a coating polymer significantly increases the stability of mechanical alignment between the microsphere and taper, accompanied by a relativity

low absorption and insertion loss of polymer packaging [28]. An additional solution to keep a high Q factor for silica microresonators and taper satisfying coupling conditions and providing improved long-term frequency stability is packaging into modules that feature temperature control by integrated Peltier elements [29].

Table 1. Results of characteristics calculations for 170 μm SiO_2 microsphere resonator versus life cycle.

Life Cycle	T	K	FWHM, MHz	Q	Q_{intr}	P_{circ}, W	I, GW/cm²	Resulting OFC
Freshly fabricated	0.13	2.1	5.2	3.7×10^7	1.2×10^8	3327	13.8	yes
After 2 months	0.64	9.0	15.7	1.2×10^7	1.2×10^8	1458	6.0	yes
After 3.5 months	0.62	8.4	50	3.9×10^6	3.6×10^7	455	1.9	no
After 4 months	0.78	16.1	96	2.0×10^6	3.5×10^7	249	1.0	no
After 4 months (repaired by Hydrogen flame)	0.74	13.3	44	4.4×10^6	6.3×10^7	538	2.2	no

3. Experimental Setup of Designed Silica Microsphere WGMR-Based Kerr-OFC as A Light Source for Application in Optical Communications

The setup used for the generation of WGMR-based Kerr-OFC is shown in Figure 2a,c. First, we prepare the tapered fiber for coupling the light into the silica microsphere. We used a non-zero dispersion-shifted fiber (NZ-DSF) patch-cable compliant with the ITU-T G.655 standard for the preparation of a tapered fiber pulling probe. In the process of the tapered fiber fabrication procedure, the tapered fiber probe was formed from two separate cut parts of an NZ-DSF compliant patch cable. The patch-cable fiber ends were cut using a fiber cleaver, cleaned, and spliced together with a commercial arc fusion splicer (Sumitomo, T-71C), ensuring a low insertion loss ≤0.01 dB. As a result, the jacket and coating of connectorized patch-cable were removed in the region of 3.8 cm, where it is intended for heat treatment.

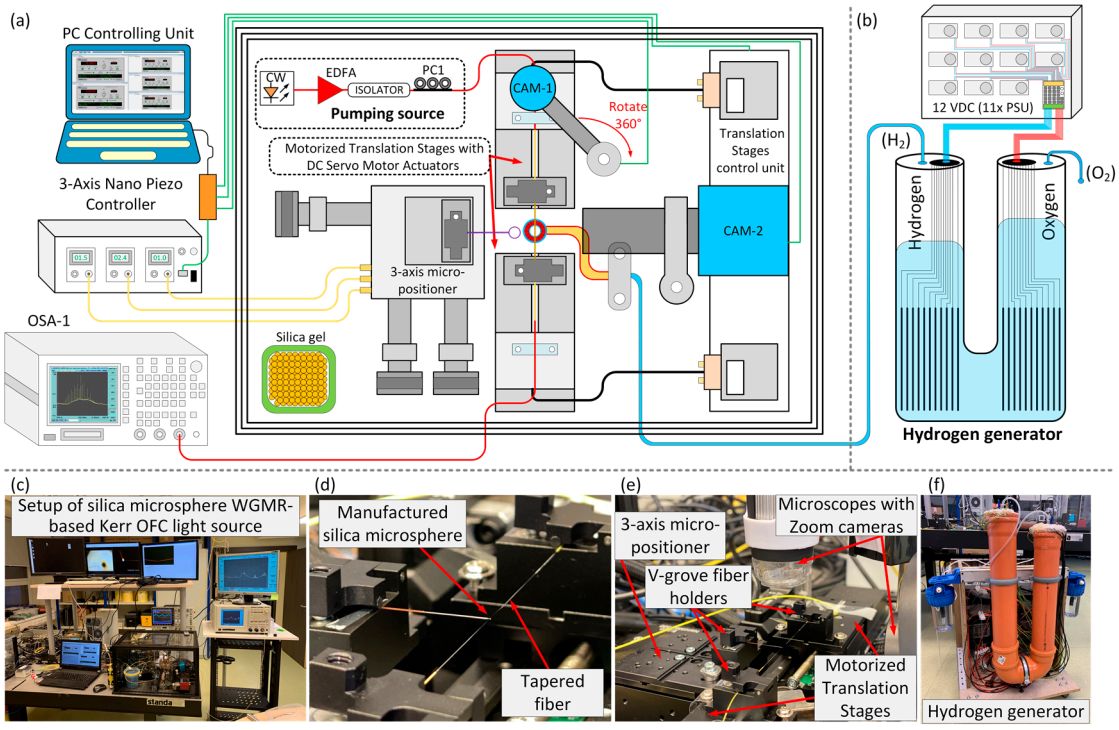

Figure 2. (**a**) Experimental setup illustrating the developed silica microsphere WGMR-based Kerr-OFC as a light source for optical communications. (**b**) Schematic of a Hydrogen generator for pure

generation of hydrogen (H_2) and oxygen (O_2) by electrolysis of water. (**c**) Captured setup of silica microsphere WGMR-based Kerr-OFC light source. (**d**) Tapered fiber and silica microsphere resonator positions inside of enclosure box for dust and airflow prevention. (**e**) The 3-axis X, Y, and Z micro-positioner stage with a built-in Piezo controller and compact, motorized translation stages together with zoom microscopes used to monitor the position of the WGMR resonator. (**f**) Captured hydrogen generator for pure hydrogen and oxygen production.

Clamps of V-grove fiber holders located on the 50 mm compact, motorized translation stages with DC servo motor actuators (Thorlabs MTS50-Z8) were used to pull the tapered fiber in both directions with a constant speed of 100 μm/s (see Figure 2a,e). Several techniques can be used to form tapered fiber through thermal heating, for instance, a ceramic tube microheater(s) consisting of a heat-resistant wire that is approximately 22 mm in length and 19 mm inner diameter and placed within the ceramic [30]; another option would be micro burners driven by propane–butane (30% propane and 70% butane) gas flows [23] or by pure hydrogen (H_2) [31], providing a high-temperature (≥1900 °C) flame. The latter setup was used in our experiments; specifically, a constant hydrogen flow of 50 mL/min from the hydrogen generator (see Figure 2b) was connected to a microburner placed between compact, motorized translation stages. For pure hydrogen generation, we use an in-house-built hydrogen generator (electrolyser) that operates by splitting the water into hydrogen and oxygen through electrolysis. The number of plates for cathode and anode is set to ×11. Each plate was driven by 12 VDC (30 A) output voltage through an 11× high-speed Schottky diodes barrier using a (220 V~50 Hz 350 W) power supply unit (PSU). As shown in Figure 2b,f, sets of 11 cathode and 11 anode plates are located in separate tubes (D = 250 mm) where the electrolysis interconnection between them was made by water and potassium hydroxide (KOH) electrolyte through a round tube transition. For the microburner, we used an in-house-built micro torch that consists of 9 cylindrical stainless-steel tubes of 0.9 mm inner diameter, allowing us to produce a low and wide flame of ~10 mm along the fiber axis [32]. The fiber position relative to the flame is a critical parameter. Therefore, the microtorch stainless-steel tube position is sprightly adjusted to the fiber's mid-point. To sustain transmission, the tapered fiber needs to be pulled adiabatically while not exceeding the delineation angle [33]. Using a ~7 mm wide hydrogen flame, we produced sub-wavelength nearly adiabatic tapers with an overall transmittance higher than 95%, as a very efficient adiabatic transfer from the single mode of the untapered fiber to the fundamental mode of the central part of the taper. The burning temperature of the hydrogen flame melted and softened the fiber slowly within the purified fiber section as a result of a tapered thicker section of 18 mm in length. It is important to mention that if the fiber ends are inclined (0.1 mrad) at the place of V-grove fiber holders, a curvature of 5 μm is intelligently formed in the melted location of the taper when the flame width is 1 mm. The angle exceeding 0.08 mrad is no longer good, as the allowable adiabatic angle is between 0.02 and 0.05 mrad [34]. Due to rapid assembly, a flame wider than 1 mm was used. The mounting of the fiber holders on one optical axis is adjusted under a microscope. The 3-axis X, Y, and Z micro-positioner stages with the built-in piezo controller were used to align the microsphere with the tapered fiber at a location slightly thicker than the taper waist to achieve the critical coupling and to minimize the coupler losses; see Figure 2d,e. Side and top view microscope cameras (CAM-1 and CAM-2) with 160× zoom lens (see Figure 2e) were used to monitor silica microsphere and tapered fiber positions to control the touchpoint of the resonator with the slightly thicker tapered fiber placed to excite the fundamental mode of the microsphere. Silica microsphere and tapered fibers, including integrated and developed components for fiber tapering and microsphere positioning, are included in an enclosure box to protect it from dust and airflows. Humidity inside the enclosure box is reduced and maintained at levels below 20% using a silica gel desiccant. The enclosure box together with pumping source components is located on a vibration isolation system breadboard table to minimize the impact of external low frequency vibrations. The setup used for the characterization of the taper fiber (see Figure 3) consists of InGaAs switchable gain amplified photo-detector (PD) λ = 800–1700

nm (Thorlabs (Bergkirchen, Germany), PDA20CS2) connected with a digital signal analyzer (DSA) used to record the received electrical signal in time and to monitor the transmission spectra from the adiabatically tapered fiber for an overall transmittance analysis used also in further telecom data transmission. A tunable λ = 1550 nm laser (Thorlabs SFL1550P) with a narrow linewidth of 50 kHz and 10 dBm output optical power is connected via a polarization controller (PC1) and used for transmission spectra measurements. The transmission spectrum was monitored during the tapering process to determine when it returns to the single-mode operation state (see Figure 4a). As shown in Figure 4a, the adiabatically tapered fiber spectrum presents single-mode (SM) operations in the beginning from 0 to 0.5 min mark and after pulling at around 3.3 min mark (represented in the red color) when the signal intensity becomes constant. SM fiber becomes multi-mode (MM) when the signal starts to propagate through the cladding (represented in the blue color).

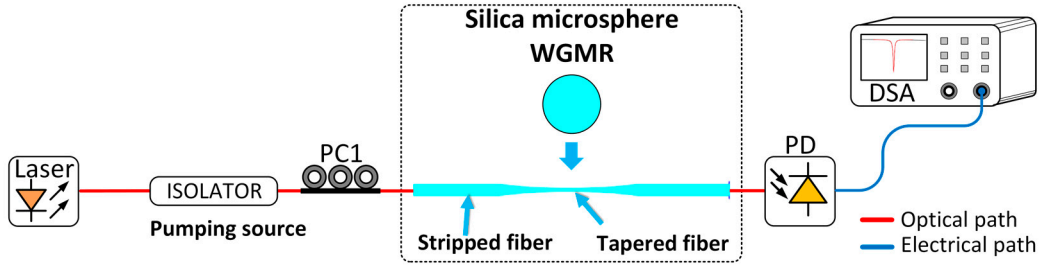

Figure 3. Experimental setup used for the characterization of the tapered fiber and silica microsphere.

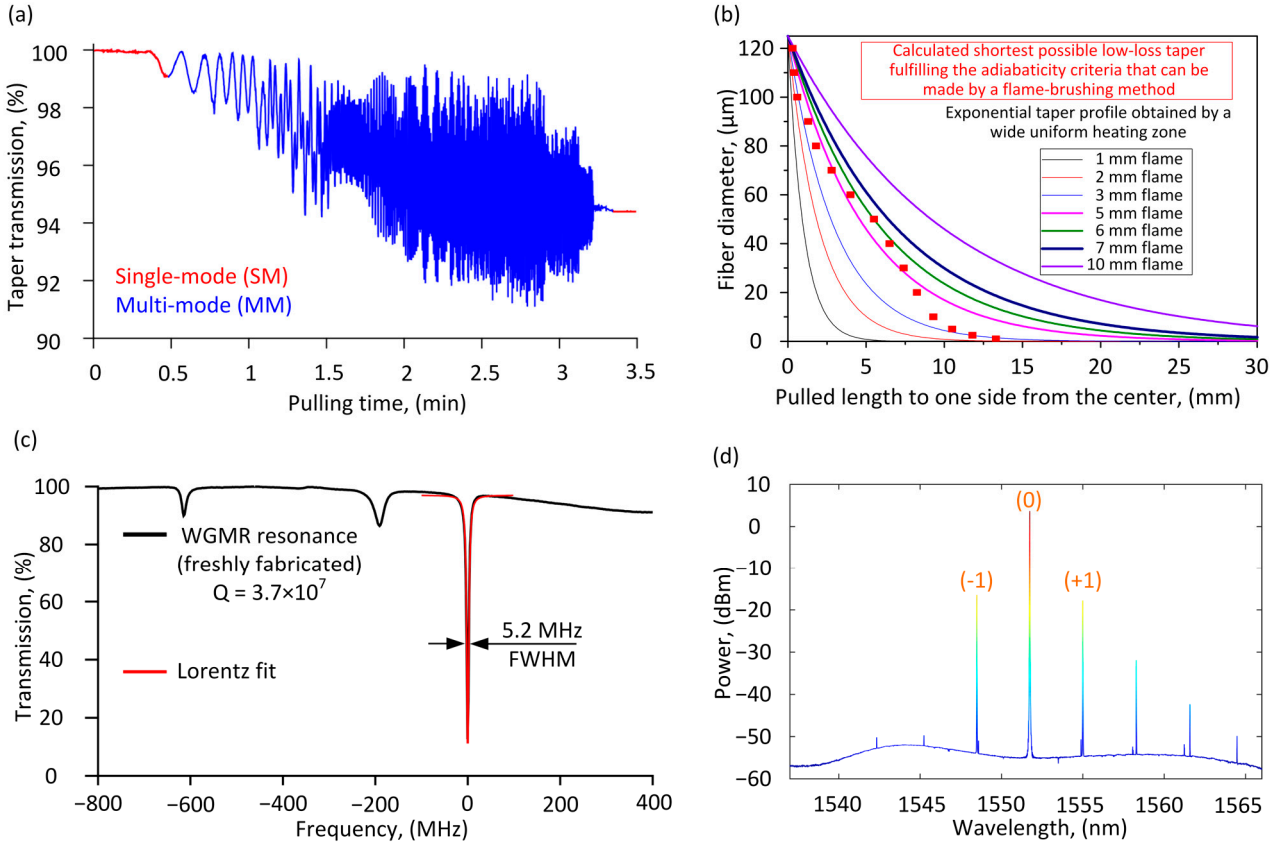

Figure 4. The characterization of the tapered fiber and its coupling conditions with the silica microsphere: (**a**) spectrum of the adiabatically tapered fiber recorded for the overall transmittance analysis and (**b**) the calculations of pulled one side fiber length at hot zone from center versus fiber

diameter at tapered section. (**c**) Experimentally observed (from the microsphere excited by the tapered fiber) WGM resonances of the Kerr-OFC at the optical C-band used for the Q factor calculation and (**d**) optical spectra of the generated silica microsphere WGMR-based Kerr-OFC comb source.

Calculations show that the hot zone's width of exponentially pulled tapered fiber should be at least 7 mm long to satisfy the adiabaticity criteria at the middle of the pulling range and to maintain high final transmission [33]. Please see the calculations of the pulled length of tapered fiber hot zone to one side from center versus fiber diameter at the tapper section in Figure 4b. The setup shown in Figure 3 also was used to determine the Q factor of the silica microsphere and to identify the best coupling condition region between the microsphere and tapered fiber used in OFC generation. The measured Q factor of the microsphere used for OFC comb generation and further telecom data transmission is 3.7×10^7 (5.2 MHz FWHM of the WGM resonance); please see Figure 4c. As shown in Figure 4c, resonances were obtained by scanning the laser over resonances while Kerr-OFC was generated with a single pumping wavelength. The silica microsphere resonator supports many modes inside the cavity, but not all modes in addition to the fundamental mode can support Kerr-OFC generation.

The pumping source for the Kerr-OFC generation consists of a continuous optical wavelength (CW) laser source (Agilent 81989A) with a linewidth of 100 kHz and +6 dBm optical output power at λ = 1551.737 nm wavelength that is directly connected to fixed output power (up to +23 dBm) erbium-doped fiber amplifier (EDFA). The light coming from the EDFA is passed through an optical isolator and PC1 to prevent back-scattering and to control the amplified signal's polarisation state before coupling it into the microsphere through the tapered fiber, providing further stability of the resulting OFC. An optical spectrum analyzer (OSA-1, Advantest Q8384) with 0.01 nm resolution and 1001 sampling points is used to monitor generated OFC as well as to measure the peak powers of generated (−1) and (+1) carriers and pumping source depicted as a carrier (0); see Figure 4d. The power instability and power distribution stability over the wavelength of the generated OFC comb carriers was not measured during this research. The generated comb carriers (−1) and (+1) over 10 h have a different performance within about a 3 dB margin; please see our previous work [9]. Silica microsphere WGMR-based Kerr-OFC light source newly generated carriers (−1) and (+1) and comb carriers followed by (+1) carrier have additional sub-carriers generated under the influence of stimulated Brillouin scattering (SBS); see Figure 4d. The SBS effect occurs due to a relatively high pumping power launched from EDFA (up to +23 dBm) in the 170 μm silica microsphere. The SBS effect appears and then disappears in the time interval for both the pumping source and the newly generated carriers on the left or right side with a constant FSR of ~10 GHz and various power levels within the time interval of about ~15 min (usually this is observed when the comb has been operated for some time). It is relatively hard to detect and predict those sub-carriers bursts because their phenomenon is unstable and changeable in time-lapse, as captured and shown in Figure 4d.

4. Experimental Setup of the Silica Microsphere WGMR-Based Kerr-OFC Light Source for Its Use in High-Speed IM/DD Short-Reach Optical Interconnects

The experimental setup is shown in Figure 5. The silica microsphere WGMR-based Kerr-OFC light source (i.e., Kerr-OFC) output 400 GHz spaced optical carriers at wavelengths λ = 1548.485 nm depicted as (−1), λ = 1554.992 nm depicted as (+1), and the pumping source at λ = 1551.737 nm depicted as (0) and having the highest achieved peak power levels (≥−15 dBm) are used to demonstrate NRZ-OOK modulated data up to 50 Gbps/λ over 2 km SMF link. As shown in Figure 5, the generated OFC carriers are sent to an optical band-pass filter (OBPF, Santec (London, UK), OTF-350), possessing a 3 dB bandwidth of 75 GHz. The OBPF is used to filter out one of the three optical carriers. An optical coupler with a 10/90 coupling ratio is used to capture the output carrier spectrum using OSA-2. It is performed for monitoring purposes and to determine carriers' wavelengths and

optical peak powers that are later used for data transmission. The filtered optical carrier is amplified by a pre-amplifier (EDFA2) that fixes the output power level for each OFC carrier. A polarization controller (PC2) is placed before the intensity Mach–Zehnder modulator (MZM, Photline (Paris, France), MX-LN40) to reduce the polarization-dependent loss. The high-speed NRZ signal is generated offline using a 2^{15}–1 long pseudorandom binary sequence (PRBS).

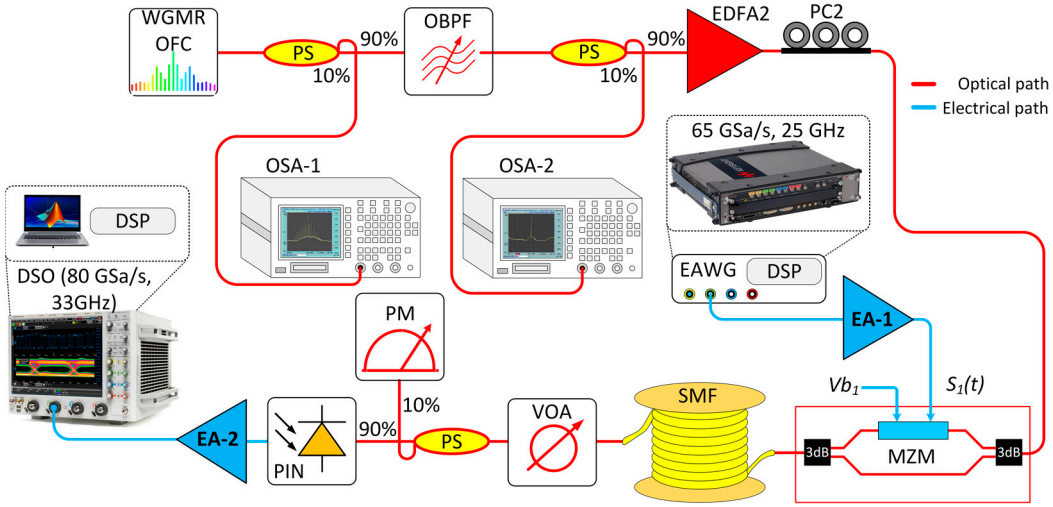

Figure 5. Experimental demonstration of the IM/DD optical interconnect relying on the in-house-built silica microsphere WGMR-based Kerr-OFC as a light source generating 400 GHz spaced optical carriers that are used for up to 50 Gbps/λ NRZ-OOK modulated signal transmission over a 2 km long SMF link.

The signal is up-sampled and filtered using a root-raised-cosine (RRC) filter having a roll-off factor of 1. At the next pre-processing stage, frequency domain pre-equalization up to 30 GHz is used to compensate for amplitude–frequency distortions and limited bandwidths (BWs) of a 65 GSa/s electrical arbitrary waveform generator (EAWG, Keysight M9502A, 25 GHz). Please observe (Figure 6) the response of an end-to-end system calibration for the optical back-to-back (OB2B) configuration.

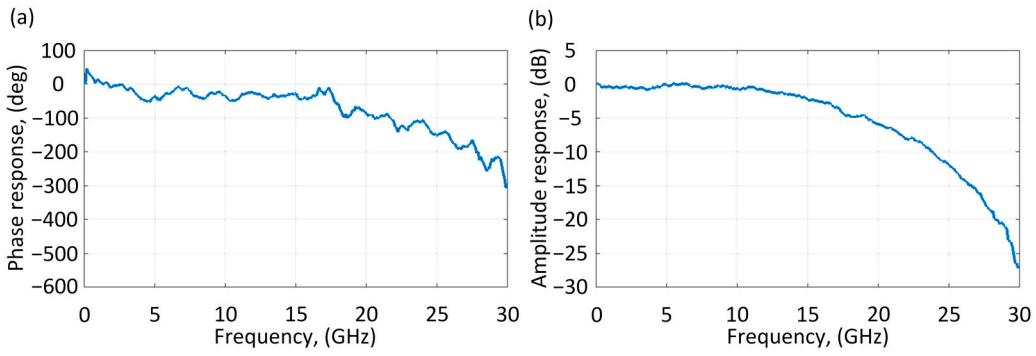

Figure 6. End-to-end system calibration using the EAWG for the OB2B configuration: (**a**) phase response and (**b**) amplitude response.

The high-speed NRZ encoded signal is loaded to the EAWG, pre-equalized, and transmitted. The generated output electrical signals are amplified by an electrical amplifier (EA-1, 38 GHz, and 29 dB gain) and fed into the $S_1(t)$ input of the MZM with a null chirp factor and having 40 GHz 3 dB bandwidth, 20 dB extinction ratio, and 9 dB insertion loss. To ensure the best possible BER performance, we adjusted a bias voltage Vb_1 of the MZM to 3.8 V. After MZM, the modulated optical signal is transmitted over a 2 km long

SMF link and passed through a variable optical attenuator (VOA) located before a photoreceiver for the power control. The photoreceiver module (PIN, Lab Buddy, DSC10H-39) consists of high optical power 50 GHz InGaAs photodiode with a 3 dB bandwidth of 50 GHz, a sensitivity of +4 dBm at BER of 10^{-12}, and responsivity of 0.5 A/W. An optical coupler with a 10/90 coupling ratio and a power meter were used before PIN to monitor the optical power level at the receiver. After optical-to-electrical conversion, the electrical signal is amplified by an electrical amplifier (EA-2, 25 GHz, 16 dB gain). Thereafter, the signal is captured by a digital storage oscilloscope (DSO, Keysight DSAZ334A, 80 GSa/s, 33 GHz). The sampled signal is processed offline using digital signal processing (DSP) consisting of a low-pass filter (LPF), clock recovery, resampling, and linear post-equalization based on a symbol-spaced adaptive decision-feedback equalizer (DFE) and bit error rate (BER) counter. Please note that BER values are obtained using bit-by-bit comparison between the transmitted and received bit sequences.

5. Experimental Results

Using the experimental setup shown in Figure 5 and described in Section 4, we make a fair comparison, showing the performance limits in terms of achievable data rates for short-reach optical interconnect applications. Our goal is to achieve a data rate that is as high as possible, even up to 60 Gbps/λ in the system that uses the implemented Kerr-OFC generated optical carriers for carrying IM/DD data. The received and sampled signal is processed offline after the reception, using a DSP routine that consists of a low-pass filter (LPF), a maximum variance timing recovery, post-equalization, and a BER counter. The LPF has a bandwidth of 0.6 times the Baud rate. That value was identified using the results data shown in Figure 7. It ensures the best possible performance after further processing. In such a case, we obtain BER as a function of the LPF_{BW}/Baud rate from 0.4 to 0.8 for NRZ-OOK signals.

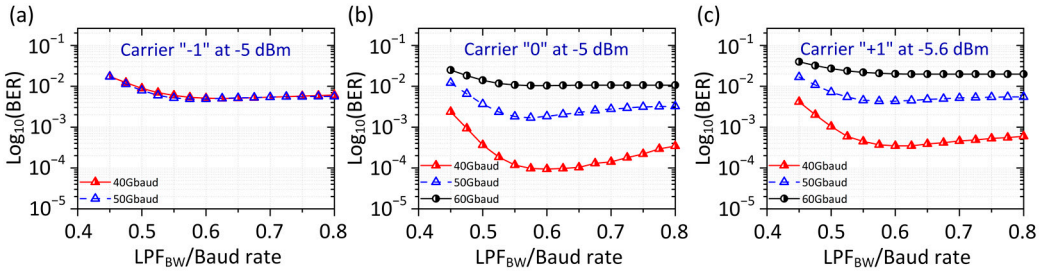

Figure 7. BER versus LPF_{bw}/Baud rate for the IM/DD communication system operating on 400 GHz spaced carriers generated by microsphere Kerr-OFC: (**a**) λ = 1548.485 depicted as carrier "−1"; (**b**) λ = 1551.737 depicted as carrier "0"; (**c**) λ = 1554.992 depicted as carrier "+1" provide NRZ-OOK signals up to 60 Gbps/λ.

The post-equalization was used to improve signal quality; we use a DFE configuration with 33 feed-forward taps (FFT) and 15 feedback taps (FBT), as well as 16 taps are used as a reference. The adaptive DFE helps to overcome the inter-symbol interference ISI in the presence of noise and bandwidth limitations. As shown in Figure 7a, 40 Gbaud and 50 Gbaud signals are almost overlapping because DFE with both feed-forward (FF) and feedback (FB) taps due to the intensity fluctuations (power instability) of carrier (−1) cannot show performance improvements in terms of high baud rate. The initial weights of the equalizer are obtained using the training data with the normalized least-mean-square (NLMS) algorithm before applying other data. A total number of 1.2 million bits are used for BER counting.

First, we analyze system performance without post-equalization. Afterward, we focus on improvements that the linear post-equalization can offer. We show BER curves and eye diagrams of the received NRZ-OOK signals after the 2 km transmission over the SMF

link. In this paper, we consider the hard-decision forward error correction (HD-FEC) with 7% overheads (OH) with a pre-FEC BER threshold at 5×10^{-3} [35]. We use the conventional BER curves showing how pre-FEC BER values change with the received optical power (ROP). We assume that all errors can be corrected for the pre-FEC BER below that threshold. As one can see in Figure 8a, the worst-performing (based on the BER value) data channel is the carrier (−1) at 1548.485 nm, yet it is capable in providing the maximum bitrate of 50 Gbps. In this sub-figure, the 60 Gbps curve is not shown because due to extremely poor BER performance, i.e., it is way beyond our defined pre-FEC BER threshold of 5×10^{-3}. The best performing (based on the BER) data channel is the pumping source carrier with a wavelength of 1551.737 nm depicted as a carrier (0). Without the post-equalization, the received 40 Gbaud and 50 Gbaud NRZ-OOK signals are mostly below the 7% HD-FEC limit for the Kerr-OFC generated carriers (−1), (0), and (+1); see Figure 8a–c. In those cases, the main limitations are a relatively low effective bandwidth of the electrical components, ISI, and the implementation penalty itself.

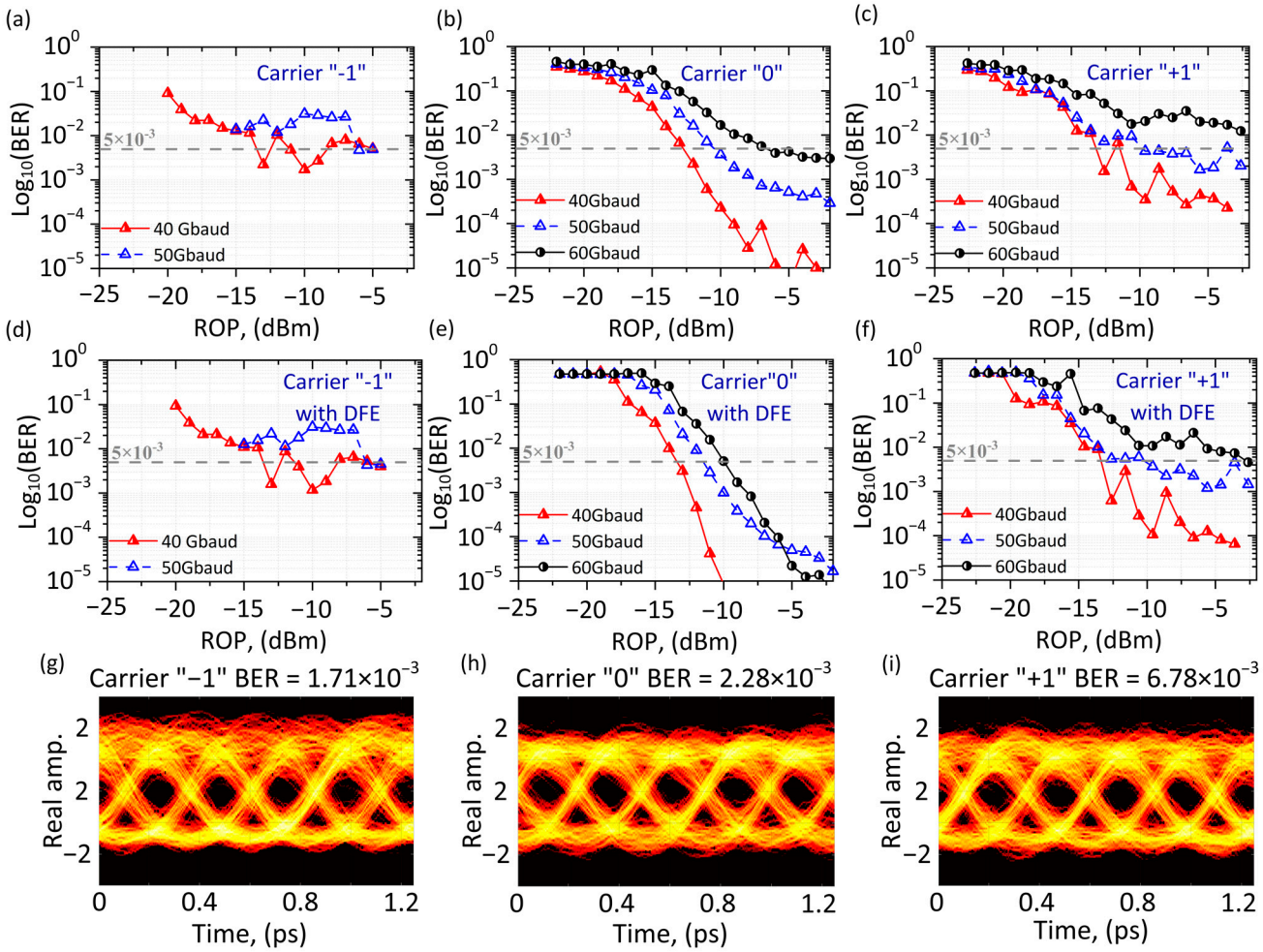

Figure 8. BER versus ROP for the IM/DD communication system where the Kerr-OFC light source carriers "−1", "0", and "+1" can be used for NZR-OOK signals transmission with baud rates up to (**a**) 50 Gbaud, (**b**) 60 Gbaud, and (**c**) 50 Gbaud without any post-equalization. If the post-equalizer with 33-FF and 15-FB taps is used, the BER is significantly improved for carriers "−1", "0", and "+1" up to (**d**) 50 Gbaud, (**e**) 60 Gbaud, and (**f**) 60 Gbaud. Received signal eye diagrams for carriers: (**g**) "−1", (**h**) "0", and (**i**) "+1" captured at ROP of −10 dBm in the 40 Gbaud case.

To achieve higher data rates, a dispersion-induced power fading must be reduced, and signal equalization must be applied to reach the BER threshold of 5×10^{-3}. We have chosen a linear equalizer for which its structure consists of 33-FF and 15-FB taps. The

number of taps is chosen in a manner that maximally improves performance by tackling the bandwidth limitations of electrical components and chromatic dispersion. The results show that such post-equalization significantly improves BER performance compared to the previous case without the post-equalization. As one can see in Figure 8e,f, post-equalization can significantly improve the signal quality for Kerr-OFC generated carriers (0) and (+1), or even enable new modulation format alternatives. However, the feed-forward equalizer, due to the intensity fluctuations of the (−1) carrier, cannot show visible performance improvement (see Figure 8a,d).

With the linear post-equalization (33-FF and 15-FB taps), BER performance is significantly improved for carrier (+1), which allows us to achieve the BER floor below the 7% HD-FEC limit for NRZ-OOK signals at 60 Gbaud. Figure 8g–i show the corresponding eye diagrams captured for modulated carriers (−1), (0), and (+1) at −10 dBm received optical power (ROP) that allows detecting signals with BER below 5×10^{-3} at 40 Gbaud.

6. Conclusions

This work is a significant achievement by experimentally demonstrating a data transmission record of 50 Gbps per λ with a silica microsphere WGMR-based Kerr-OFC light source. In this experiment, we have designed and demonstrated the silica microsphere WGMR-based Kerr-OFC built in-house and used as a light source for data center interconnects (DCIs). The Kerr-OFC consists of several carriers spaced 400 GHz apart together with powerful pre- and post-linear equalization techniques, such as a linear symbol-spaced adaptive decision-feedback equalizer (DFE) with feed-forward (FF), and feedback (FB) taps provide an alternative to ensure low-cost and low-complexity IM/DD schemes for the transmission of NRZ-OOK modulated signals over 2 km SMF links. The obtained results show that pre- and post-equalization techniques allow overcoming the ISI and help recover the signal from distortions caused by limited bandwidth, enabling higher data-rate alternatives to intra-DCIs. Without post-equalization, the received 40 Gbaud and 50 Gbaud NRZ-OOK signals are below the 7% HD-FEC limit for Kerr-OFC generated carriers (−1), (0), and (+1). The linear post-equalization, namely 33-FF and 15-FB taps, improves BER performance for carrier (+1), which allows us to achieve the BER floor below the 7% HD-FEC limit even for NRZ-OOK signals at 60 Gbaud.

Author Contributions: Conceptualization, T.S., J.A. and. O.O.; methodology, T.S.; software, T.S., J.A., E.A.A., A.V.A., S.S., R.B., X.P. and V.B.; validation, A.U., E.A.A., S.S. and V.B.; formal analysis, A.U., E.A.A., S.S., I.B., R.B. and V.B.; investigation, T.S. and J.A.; resources, T.S., S.S., E.A.A., A.V.A., J.A. and V.B.; data curation, T.S.; writing—original draft preparation, T.S., A.U., S.S., I.B., J.A., E.A.A. and O.O.; writing—review and editing, T.S., J.A., O.O., A.V.A., E.A.A., I.B., R.B., X.P., A.U., J.P., S.S. and V.B.; visualization, T.S., I.B., J.A. and O.O.; supervision, J.A., S.S., O.O. and V.B.; project administration, T.S., S.S., J.A. and V.B.; funding acquisition, T.S., S.S., E.A.A., A.V.A. and V.B. All authors have read and agreed to the published version of the manuscript.

Funding: This research was funded by European Regional Development Fund (1.1.1.1/18/A/155); Ministry of Science and Higher Education of the Russian Federation (075-15-2021-633); Russian Science Foundation (20-72-10188).

Institutional Review Board Statement: Not applicable.

Informed Consent Statement: Not applicable.

Data Availability Statement: Not applicable.

Acknowledgments: This research was funded by the European Regional Development Fund project No. 1.1.1.1/18/A/155 "Development of optical frequency comb generator based on a whispering gallery mode microresonator and its applications in telecommunications". The taper fiber preparation was supported by the European Social Fund within project number No. 8.2.2.0/20/I/008 and by the the Austrian Science Fund FWF within the DK-ALM W1259-N27. The development of the program for the optical fusion splicer was funded by the Mega-grant of the Ministry of Science and Higher Education of the Russian Federation, Contract No. 075-15-2021-633. The fabrication of test samples of microspheres was funded by the Russian Science Foundation, Grant No. 20-72-10188.

Communication Technologies Research Center, Riga Technical University (RTU) acknowledges support from RTU Science Support Fund.

Conflicts of Interest: The authors declare no conflict of interest.

References

1. Torres-Company, V.; Weiner, A.M. Optical frequency comb technology for ultra-broadband radio-frequency photonics. *Laser Photonics Rev.* **2014**, *8*, 368–393. https://doi.org/10.1002/lpor.201300126.
2. Ludlow, A.D.; Boyd, M.M.; Ye, J.; Peik, E.; Schmidt, P.O. Optical atomic clocks. *Rev. Mod. Phys.* **2015**, *87*, 637–701. https://doi.org/10.1103/RevModPhys.87.637.
3. Kwon, D.; Jeon, I.; Lee, W.K.; Heo, M.S.; Kim, J. Generation of multiple ultrastable optical frequency combs from an all-fiber photonic platform. *Sci. Adv.* **2020**, *6*, eaax4457. https://doi.org/10.1126/sciadv.aax4457.
4. Predehl, K.; Grosche, G.; Raupach, S.M.F.; Droste, S.; Terra, O.; Alnis, J.; Legero, Th.; Hänsch, T.W.; Udem, T.; Holzwarth, R.; Schnatz, H.; A 920-km optical fiber link for frequency metrology at the 19th decimal place. *Science* **2012**, *336*, 441–444. https://doi.org/10.1126/science.1218442.
5. Adler, F.; Thorpe, M.J.; Cossel, K.C.; Ye, J. Cavity-enhanced direct frequency comb spectroscopy: Technology and applications. Annu. *Rev. Anal. Chem.* **2010**, *3*, 175–205. https://doi.org/10.1146/annurev-anchem-060908-155248.
6. Guay, P.; Hébert, N.B.; Michaud-Belleau, V.; Lancaster, D.G.; Genest, J. Free-running optical frequency combs for remote sensing. In *Optical Sensors and Sensing Congress (ES, FTS, HISE, Sensors), OSA Technical Digest*; Optica Publishing Group: Washington, DC, USA, 2019; Paper ETu3A.6. https://doi.org/10.1364/ES.2019.ETu3A.6.
7. Lu, H.H.; Weiner, A.M.; Lougovski, P.; Lukens, J.M. Quantum Information Processing with Frequency-Comb Qudits. *IEEE Photon. Technol. Lett.* **2019**, *31*, 1858–1861. https://doi.org/10.1109/LPT.2019.2942136.
8. Pfeifle, J.; Brasch, V.; Lauermann, M.; Yimin, Y.; Wegner, D.; Herr, T.; Hartinger, K.; Schindler, P.; Li, J.; Hillerkuss, D.; et al. Coherent terabit communications with microresonator Kerr frequency combs. *Nat. Photon* **2014**, *8*, 375–380. https://doi.org/10.1038/nphoton.2014.57.
9. Salgals, T.; Alnis, J.; Murnieks, R.; Brice, I.; Porins, J.; Andrianov, A.V.; Anashkina, E.A.; Spolitis, S.; Bobrovs, V. Demonstration of a fiber optical communication system employing a silica microsphere-based OFC source. *Opt. Express* **2021**, *29*, 10903. https://doi.org/10.1364/OE.419546.
10. Kong, D.; Xin, H.; Kim, K.; Liu, Y.; Oxenløwe, L.K.; Dong, P.; Hu, H. Intra-Datacenter Interconnects With a Serialized Silicon Optical Frequency Comb Modulator. *J. Lightwave Technol.* **2020**, *38*, 4677–4682. https://doi.org/10.1109/JLT.2020.2996410.
11. Pang, X.; Udalcovs, A.; Schatz, R.; Bobrovs, V.; Jacobsen, G.; Popov, S.; Ozolins, O. Short Reach Communication Technologies for Client-Side Optics Beyond 400 Gbps. *IEEE Photon. Technol. Lett.* **2021**, *33*, 1046–1049. https://doi.org/10.1109/LPT.2021.3078255.
12. Spolitis, S.; Murnieks, R.; Skladova, L.; Salgals, T.; Andrianov, A.V.; Marisova, M.P.; Leuchs, G.; Anashkina, E.A.; Bobrovs, V. IM/DD WDM-PON Communication System Based on Optical Frequency Comb Generated in Silica Whispering Gallery Mode Resonator, *IEEE Access* **2021**, *9*, 66335–66345. https://doi.org/10.1109/ACCESS.2021.3076411.
13. Hu, H.; Oxenløwe, L.K. Chip-based optical frequency combs for high-capacity optical communications. *Nanophotonics* **2021**, *10*, 1367–1385. https://doi.org/10.1515/nanoph-2020-0561.
14. Wu, R.; Supradeepa, V.R.; Long, C.M.; Leaird, D.E.; Weiner, A.M. Generation of very flat optical frequency combs from continuous-wave lasers using cascaded intensity and phase modulators driven by tailored radio frequency waveforms. *Opt. Lett.* **2010**, *35*, 3234. https://doi.org/10.1364/OL.35.003234.
15. Chembo, Y.K. Kerr optical frequency combs: Theory, applications and perspective. *Nanophotonics* **2016**, *5*, 214–230. https://doi.org/10.1515/nanoph-2016-0013.
16. Kippenberg, T.J.; Gaeta, A.L.; Lipson, M.; Gorodetsky, M.L. Dissipative Kerr solitons in optical microresonators. *Science* **2018**, *361*, eaan8083. https://doi.org/10.1126/science.aan8083.
17. Lee, S.H.; Oh, D.Y.; Yang, Q.-F.; Shen, B.; Wang, H.; Yang, K.Y.; Lai, Y.-H.; Yi, X.; Li, X.; Vahala, K. Towards visible soliton microcomb generation. *Nat. Commun.* **2017**, *8*, 1295. https://doi.org/10.1038/s41467-017-01473-9.
18. Anashkina, E.A.; Marisova, M.P.; Salgals, T.; Alnis, J.; Lyashuk, I.; Leuchs, G.; Spolitis, S.; Bobrovs, V.; Andrianov, A.V. Optical Frequency Combs Generated in Silica Microspheres in the Telecommunication C-, U-, and E-Bands. *Photonics* **2021**, *8*, 345. https://doi.org/10.3390/photonics8090345.
19. Salgals, T.; Ostrovskis, A.; Ipatovs, A.; Bobrovs, V.; Spolitis, S. Hybrid ARoF-WDM PON Infrastructure for 5G Millimeter-wave Interface and Broadband Internet Service. In Proceedings of the Photonics & Electromagnetics Research Symposium-Fall (PIERS-Fall), Xiamen, China, 17–20 December 2019. https://doi.org/10.1109/PIERS-Fall48861.2019.9021479.
20. Anashkina, E.A.; Marisova, M.P.; Andrianov, A.V.; Akhmedzhanov, R.A.; Murnieks, R.; Tokman, M.D.; Skladova, L.; Oladyshkin, I.V.; Salgals, T.; Lyashuk, I.; et al. Microsphere-Based Optical Frequency Comb Generator for 200 GHz Spaced WDM Data Transmission System. *Photonics* **2020**, *7*, 72. https://doi.org/10.3390/photonics7030072.
21. Anashkina, E.A.; Bobrovs, V.; Salgals, T.; Brice, I.; Alnis, J.; Andrianov, A.V. Kerr Optical Frequency Combs With Multi-FSR Mode Spacing in Silica Microspheres. *IEEE Photon. Technol. Lett.* **2021**, *33*, 453. https://doi.org/10.1109/LPT.2021.3068373.

22. Udalcovs, A.; Salgals, T.; Zhang, L.; Pang, X.; Djupsjöbacka, A.; Spolitis, S.; Bobrovs, V.; Popov, S.; Ozolins, O. Optical Power Budget of 25+ Gbps IM/DD PON with Digital Signal Post-Equalization. *Appl. Sci.* **2020**, *10*, 6106. https://doi.org/10.3390/app10176106.
23. Andrianov, A.V.; Anashkina, E.A. Single-mode silica microsphere Raman laser tunable in the U-band and beyond. *Results Phys.* **2020**, *17*, 103084. https://doi.org/10.1016/j.rinp.2020.103084.
24. Gorodetsky, M.L.; Savchenkov, A.A.; Ilchenko, V.S. Ultimate Q of optical microsphere resonators. *Opt. Lett.* **1996**, *21*, 453. https://doi.org/10.1364/OL.21.000453.
25. Kovach, A.; Chen, D.; He, J.; Choi, H.; Dogan, A.H.; Ghasemkhani, M.; Taheri, H.; Armani, A.M. Emerging material systems for integrated optical Kerr frequency combs. *Adv. Opt. Photon.* **2020**, *12*, 135. https://doi.org/10.1364/AOP.376924.
26. Del'Haye, P.; Schliesser, A.; Arcizet, O.; Wilken, T.; Holzwarth, R.; Kippenberg, T.J. Optical frequency comb generation from a monolithic microresonator. *Nature* **2007**, *450*, 1214–1217. https://doi.org/10.1038/nature06401.
27. Spillane, S.M.; Kippenberg, T.J.; Painter, O.J.; Vahala, K.J. Ideality in a Fiber-Taper-Coupled Microresonator System for Application to Cavity Quantum Electrodynamics. *Phys. Rev. Lett.* **2003**, *91*, 043902. https://doi.org/10.1103/PhysRevLett.91.043902.
28. Wang, P.; Ding, M.; Murugan, G.S.; Bo, L.; Guan, C.; Semenova, Y.; Wu, Q.; Farrell, G.; Brambilla, G. Packaged, high-Q, microsphere-resonator-based add–drop filter. *Opt. Lett.* **2014**, *39*, 5208. https://doi.org/10.1364/OL.39.005208.
29. Suh, M.; Wang, C.Y.; Johnson, C.; Vahala, K.J. Directly pumped 10 GHz microcomb modules from low-power diode lasers. *Opt. Lett.* **2019**, *44*, 1841. https://doi.org/10.1364/OL.44.001841.
30. Yu, J.; Lewis, E.; Farrell, G.; Wang. P. Compound Glass Microsphere Resonator Devices. *Micromachines* **2018**, *9*, 356. https://doi.org/10.3390/mi9070356.
31. Svela, A.; Silver, J.; Del Bino, L.; Zhang, S.; Woodley, M.T.M.; Vanner, M.R.; Del'Haye, P. Coherent suppression of backscattering in optical microresonators, *Light Sci Appl* **2020**, *9*, 204. https://doi.org/10.1038/s41377-020-00440-2.
32. Orucevic, F., Seguin, V.L.; Hare, J. Transmittance and near-field characterization of sub-wavelength tapered optical fibers. *Opt. Express* **2007**, *15*, 13624. https://doi.org/10.1364/OE.15.013624.
33. Nagai, R.; Aoki, T. Ultra-low-loss tapered optical fibers with minimal lengths. *Opt. Express* **2014**, *22*, 28427. https://doi.org/10.1364/OE.22.028427.
34. Tiecke, T.G.; Nayak, K.P.; Thompson, J.D.; Peyronel, T.; de Leon, N.P.; Vuletić, V.; Lukin, M.D. Efficient fiber-optical interface for nanophotonic devices. *Optica* **2015**, *2*, 70. https://doi.org/10.1364/OPTICA.2.000070.
35. Jian, Y., Pfister, H.D.; Narayanan, K.R.; Raghu, R.; Mazahreh, R. In Iterative hard-decision decoding of braided BCH codes for high-speed optical communication. In Proceedings of the 2013 IEEE Global Communications Conference (GLOBECOM), Atlanta, GA, USA, 9–13 December 2013. https://doi.org/10.1109/GLOCOM.2013.6831429.